CB reconstruction for the 3-sin trajectory with transverse truncation

Nicolas Gindrier, Laurent Desbat, Rolf Clackdoyle

CB reconstruction for the 3-sin trajectory with transverse truncation

Nicolas Gindrier[1], Laurent Desbat[1], and Rolf Clackdoyle[1]

[1]TIMC-IMAG laboratory, CNRS UMR 5525 and Univ. Grenoble Alpes 38000 Grenoble, France

Abstract In cone-beam tomography Differentiated BackProjection method (DBP) is a suitable approach for image reconstruction from truncated projections. However, the reconstruction of a point with this method is possible only if the point lies on a chord connecting two source positions of the x-ray source trajectory. Using an approach initially proposed for the reverse helix with axial truncation, we present a configuration and its associated (theoretical) reconstruction method to deal with points which do not lie on any chord of the 3-sin trajectory (sine on a cylinder of period $2\pi/3$) and with transversely truncated projections.

1 Introduction

Cone beam (CB) geometry is an important part of the computed tomography. A main result of CB tomography comes from Tuy [1] and Finch [2]. They prove that for an X-ray source trajectory which is bounded and connected, an exact reconstruction is only possible within the convex hull of this trajectory. Moreover, in this case, the Tuy condition says exact reconstruction is possible if there is no data truncation. FOV is defined as follows in our article: the measured rays for each projection are exactly those that intersect the FOV. In this article, the FOV will be a $\boldsymbol{e}_z$-axis cylinder and we deal with *transverse truncation*, appearing when the detector is not large enough (the FOV and the object intersect at their sides). To manage this kind of reconstruction, the Differentiated BackProjection method (DBP) [3] is suitable, for example in [4] for the helix trajectory. Yet this method requires that each point of the object Ω_O to be reconstructed is intersected by a chord (a line segment linking two source points of the X-ray source trajectory).
However, many trajectories have points within their convex hull which are not intersected by a chord. For example, this is the case for the reverse helix [5] and for the 3-sin trajectory, which is a sinusoid on a cylinder, defined by:

$$S \overset{\text{def}}{=} \{(R\cos\lambda, R\sin\lambda, H\cos(3\lambda)), \lambda \in [0, 2\pi)\} \quad (1)$$

with $R > 0$, $H > 0$, see Fig. 1, *left*. Nevertheless, [6] shows by numerical methods that exact reconstruction with transverse truncation appears to be possible even in some regions which are not intersected by chords. Moreover, S has a convex hull bigger than that of the saddle trajectory (a 2-sin trajectory more extensively studied in the literature [7]), which is why we find it useful to study. We write Ω_S for the convex hull (Fig. 1, *right*) and $C_S(\subset \Omega_S)$ for the union of all chords c for the 3-sin trajectory S, and $N_S \overset{\text{def}}{=} \Omega_S \setminus C_S$.
The article [5], treating the reverse helix case, explains how to perform reconstructions dealing with some points in the convex hull which are not lying on a chord and axial truncation (the article [8], published at the same time, works on the same point and proposes a similar approach, except for the last step). Inspired by the method of [5], the goal of this article is to describe and to test one configuration for the trajectory S, where it is possible to reconstruct $\Omega_{\text{in}} \overset{\text{def}}{=} \text{FOV} \cap \Omega_O \cap N_S$ despite transverse truncation. To do this, the next section analyses and describes the regions C_S and N_S. Section 3 describes the reconstruction principles and a computer simulation study is presented in section 4. We end with a short discussion and conclusion.

2 The 3-sin trajectory

2.1 Union of chords

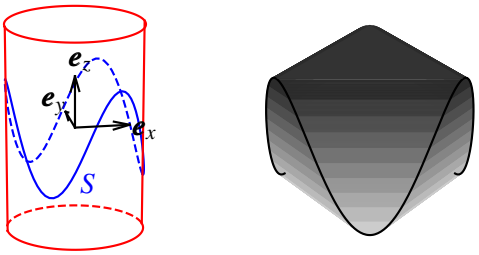

Figure 1: *Left:* the 3-sin trajectory S, which is a sinusoid on a cylinder. *Right:* the 3-sin trajectory with its convex hull Ω_S. (The shades of grey vary according to the height).

To build the union of chords C_S of the 3-sin trajectory, it is useful to consider the intersection between the trajectory and a horizontal plane $\Pi_{\tilde{z}}$ with equation $z = \tilde{z}$, where $-H \leq \tilde{z} \leq H$, illustrated in Fig. 2. The angles in this figure are:

$$\begin{aligned} \lambda_A &= -\frac{1}{3}\arccos(\tilde{z}/H) & \lambda_B &= \frac{1}{3}\arccos(\tilde{z}/H) \\ \lambda_C &= \lambda_A + \frac{2\pi}{3} & \lambda_D &= \lambda_B + \frac{2\pi}{3} \\ \lambda_E &= \lambda_A + \frac{4\pi}{3} & \lambda_F &= \lambda_B + \frac{4\pi}{3} \end{aligned} \quad (2)$$

We let $\boldsymbol{S}_A$ denote $\boldsymbol{S}_{\lambda_A}$. The aim is to show that each point of the hexagon of Fig. 2 (*right*) is intersected by a chord, except points in the central triangle (defined by the intersection of the line segments $[\boldsymbol{S}_C, \boldsymbol{S}_F]$, $[\boldsymbol{S}_D, \boldsymbol{S}_A]$ and $[\boldsymbol{S}_E, \boldsymbol{S}_B]$). Considering Fig. 3 and with equations (1) and (2), we see chords $c_1(\tilde{z})$ (linking $\boldsymbol{S}_D$ to $\boldsymbol{S}_E$ for $\tilde{z} \in [0, H]$) and $\bar{c}_1(\tilde{z})$ (linking $\boldsymbol{S}_F$ to $\boldsymbol{S}_C$ for $\tilde{z} \in [0, H]$) move (and meet when $\tilde{z} = H$), continuously approaching with respect to increasing $\tilde{z}$, for $\tilde{z} \in [0, H]$. The chord $c_2(\tilde{z})$, where $\tilde{z} \in [-H, 0]$, moves continuously with

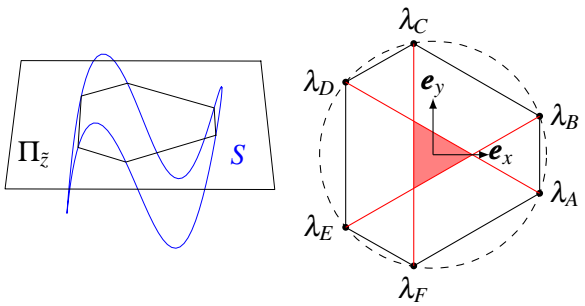

Figure 2: Intersection between a horizontal plane $\Pi_{\tilde{z}}$ and S (with the intersection points linked). *Right:* The dashed circle is the projection of S on $\Pi_{\tilde{z}}$. The red and black lines are chords of S contained in this plane $\Pi_{\tilde{z}}$. This section shows that all points contained in the black polygon, but outside the red triangle, are intersected by a chord.

respect to decreasing $\tilde{z}$ until $c_2(-H) = \boldsymbol{S}_\pi$. With the union of all chords $c_1(\tilde{z})$ and $\bar{c}_1(\tilde{z})$ for $\tilde{z} \in [0,H]$ and all chords $c_2(\tilde{z})$ for $\tilde{z} \in [-H,0]$, a surface can be created (see Fig. 4, *right*). Let's note that the 3-sin trajectory is invariant through a rotation of $2\pi/3$ around the $\boldsymbol{e}_z$-axis and is invariant through a rotation of $\pi/3$ (around the same axis) then a symmetry with respect to the plane $(\boldsymbol{e}_x, \boldsymbol{e}_y)$. With these invariances it is possible to create six similar surfaces as described previously (see Fig. 4, *left*). By adapting the proof of [7] (appendix A.2), it is possible to prove that each point between these two surfaces lies on a chord, i.e. if it exists two points $\boldsymbol{x}' = (x,y,z')$ and $\boldsymbol{x}'' = (x,y,z'')$, $z' < z''$, each intersected by a chord, then each point $\boldsymbol{x} = (x,y,z)$, with $z' < z < z''$, is also intersected by a chord. To finish the construction of C_S we must match $\boldsymbol{x}'$ and $\boldsymbol{x}''$ points, being at the union of the six surfaces, to ensure that each point within the volume of this union is intersected by a chord.

We define the blue surfaces as the surfaces generated by the chords c_1 ($[\boldsymbol{S}_D\boldsymbol{S}_E]$, $[\boldsymbol{S}_C\boldsymbol{S}_B]$ and $[\boldsymbol{S}_F\boldsymbol{S}_A]$ for $\tilde{z} \in [0,H]$, $[\boldsymbol{S}_E\boldsymbol{S}_F]$, $[\boldsymbol{S}_B\boldsymbol{S}_A]$ and $[\boldsymbol{S}_C\boldsymbol{S}_D]$ for $\tilde{z} \in [-H,0]$) and $\bar{c}_1$ ($[\boldsymbol{S}_C\boldsymbol{S}_F]$, $[\boldsymbol{S}_E\boldsymbol{S}_B]$ and $[\boldsymbol{S}_D\boldsymbol{S}_A]$). The red surfaces are defined by the surfaces generated by the chords c_2 ($[\boldsymbol{S}_D\boldsymbol{S}_E]$, $[\boldsymbol{S}_C\boldsymbol{S}_B]$ and $[\boldsymbol{S}_F\boldsymbol{S}_A]$ for $\tilde{z} \in [-H,0]$, $[\boldsymbol{S}_E\boldsymbol{S}_F]$, $[\boldsymbol{S}_B\boldsymbol{S}_A]$ and $[\boldsymbol{S}_C\boldsymbol{S}_D]$ for $\tilde{z} \in [0,H]$)(see Fig. 4). For this section each projection will be an orthogonal projection onto the plane $(\boldsymbol{e}_x, \boldsymbol{e}_y)$ (which is the plane Π_0). The intersection of the projections of the blue surfaces covers the regular hexagon defined by the convex hull of the intersection between Π_0 and S (see Fig. 3 and 5). Then a point "between" two blue surfaces (one above and one below Π_0) and whose projection is in the hexagon is intersected by a chord. A point whose projection is in the region between the hexagon defined above and the circle of radius R is intersected by a chord if it is "between" a red surface and a blue surface on the same side of Π_0. The set of points intersected by a chord is C_S, illustrated in Fig. 7, *left*.

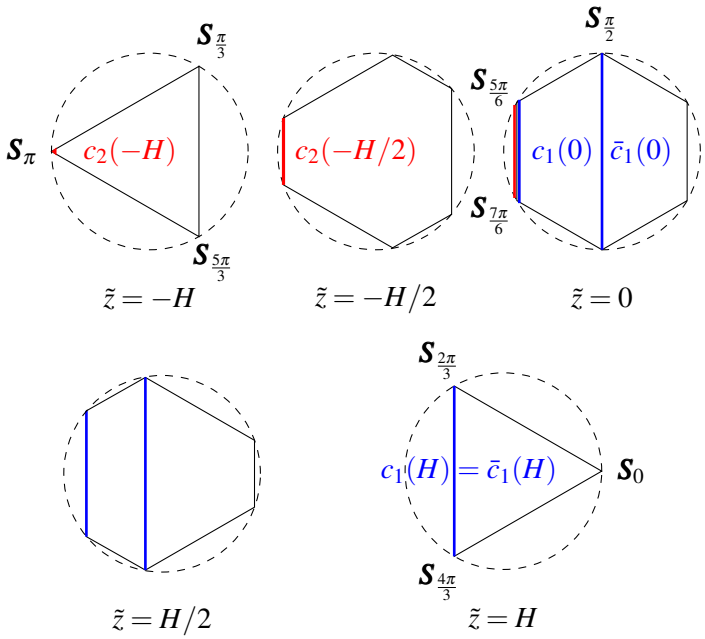

Figure 3: Different chords contained in some horizontal planes. The blue chords, defined for $\tilde{z} \geq 0$, are the chords $c_1(\tilde{z})$ (linking $\boldsymbol{S}_E$ to $\boldsymbol{S}_D$ for $\tilde{z} \geq 0$) and $\bar{c}_1(\tilde{z})$ (linking $\boldsymbol{S}_F$ to $\boldsymbol{S}_C$) and are parallel (and even merged for $\tilde{z} = H$.). The red chord is $c_2(\tilde{z})$ (linking $\boldsymbol{S}_E$ to $\boldsymbol{S}_D$ for $\tilde{z} \leq 0$). The union of these chords, for all $\tilde{z} \in [-H,H]$ is drawn Fig. 4.

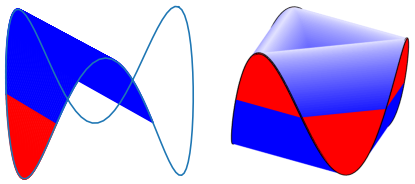

Figure 4: *Left:* One surface created for chords described Fig. 3. *Right:* The union of six surfaces from the left figure, using the invariances of the 3-sin trajectory.

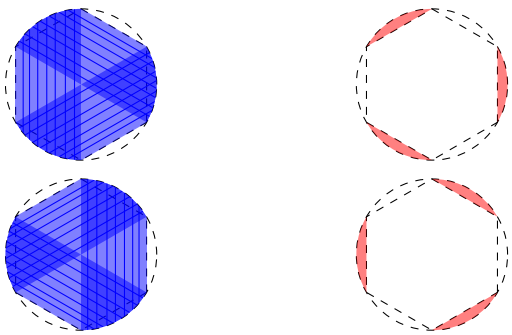

Figure 5: Orthogonal projections on the plane $(\boldsymbol{e}_x, \boldsymbol{e}_y)$ of the red and blue surfaces. *Top:* Surfaces defined for $\tilde{z} \geq 0$. *Bottom:* Surfaces defined for $\tilde{z} < 0$. The dashed hexagon links the points of the intersection between S and Π_0.

2.2 Region without chords

We have defined C_S, but to be complete now we must be sure that no chords intersect a point in the central triangle or equivalently we construct region N_S. (see Fig. 2). Considering a horizontal plane $\Pi_{\tilde{z}}$, $\tilde{z} > 0$, we cut S into several pieces s (short pieces, above $\Pi_{\tilde{z}}$) and l (long pieces, under $\Pi_{\tilde{z}}$), see Fig. 6 (for example s_1 is the piece of the trajectory linking $\boldsymbol{S}_A$ to $\boldsymbol{S}_B$). We study chords linking these pieces. There are four cases: chords linking s_1 to l_1 (directly opposite), s_1 to l_2 or l_3 ("l" to "s" but not directly opposite), s_1 to s_2 or s_3 ("s" to "s") and l_1 to l_2 or l_3 ("l" to "l"). It is clear that chords linking s_1 to l_2 do not intersect the central triangle. Chords linking s_1 to s_2 (resp. l_1 to l_2) are above (resp. below) $\Pi_{\tilde{z}}$. The last case (chords linking s_1 to l_1), is more complicated, and an analytic approach would be tedious. We show some numerically calculated intersections between these chords and $\Pi_{\tilde{z}}$ in Fig. 6 that suggest that all such intersections occur outside the triangle.

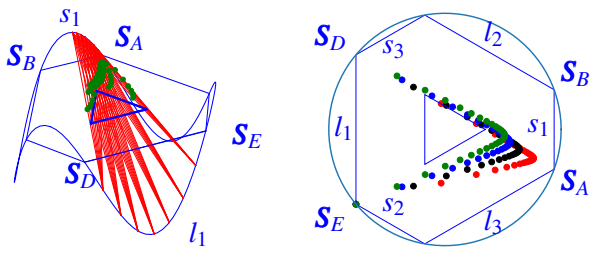

Figure 6: Chords for some values of $\lambda_1 \in [\lambda_A, \frac{\lambda_A+\lambda_B}{2}]$ (half of the s_1 piece) and $\lambda_2 \in [\lambda_D, \lambda_E]$ (l_1 piece) and intersections for the plane $\Pi_{\tilde{z}}$, $\tilde{z} = H/2$. *Right:* Intersections for four values of λ_1.

From equations (1) and (2) we are able to draw the central triangles for each $\tilde{z} \in [-H, H]$ and build an illustration of N_S, as shown in Fig. 7, *right*.

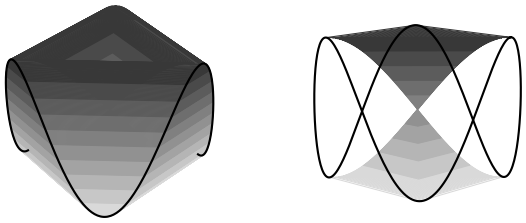

Figure 7: *Left:* The union of chords of S: C_S. *Right:* The set of points of Ω_S which are not intersected by a chord: N_S. (The shades of grey vary according to the height).

3 Reconstruction

3.1 General method

The regions Ω_O and FOV are assumed known, and C_S and N_S have been previously calculated. We can summarize the reconstruction approach in four steps:

1. Reconstruction of $\Omega_{\text{DBP}} \subseteq \text{FOV} \cap \Omega_O \cap C_S$ with the DBP method, where Ω_{DBP} is the region where DBP is possible

2. Reprojection of reconstructed points (cone-beam projections of the new object reconstructed in the region Ω_{DBP})

3. Subtraction of reprojections from the original cone-beam data, to present a new reconstruction problem with a smaller object, defined on the region $\Omega_O \setminus \Omega_{\text{DBP}} = \Omega_{\text{in}} \cup \Omega_{\text{out}}$, with $\Omega_{\text{out}} \overset{\text{def}}{=} \Omega_O \setminus (\Omega_{\text{DBP}} \cup \Omega_{\text{in}})$(the regions Ω_{DBP}, Ω_{in} and Ω_{out} are mutually disjoint)

4. For reconstruction to be possible, the new configuration must be a problem without truncation satisfying Tuy condition: reconstruction of Ω_{in} by any of the various methods for cone-beam reconstruction from non-truncated projections (e.g. [1], [9], [10]...).

However, in order to apply this method, two points must be taken into account. Firstly, the DBP method does not generally allow reconstruction in the whole region $\text{FOV} \cap \Omega_O \cap C_S$ because although the necessary Hilbert transforms can be formed along these chords, there are further geometric conditions required for Hilbert inversion (more precisely, we consider methods that guarantee the existence, stability and uniqueness of the inversion, so called 1-sided and 2-sided inverse Hilbert transforms [11]). Thus the Ω_{DBP} region must be carefully identified. Secondly, there must be no *contaminated lines*, which are defined as measured lines of Ω_{in} intersecting Ω_{out}. The region Ω_{out} could then be removed from the reconstruction problem. Note that it would not be possible to reconstruct the part of the Ω_{out} region being outside the FOV. If there are contaminated lines this approach to reconstruction of Ω_{in} fails.

3.2 Configuration proposed

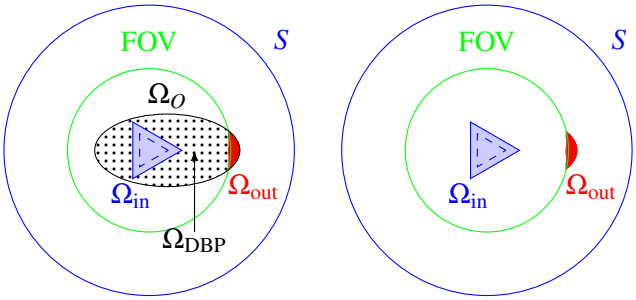

Figure 8: Top view of the considered configuration. The dashed blue triangle (resp. biggest blue triangle) delimits the intersection of N_S with the horizontal plane $z = 12$mm (resp. $z = 20$mm). A zoom on Ω_{out} is done Fig. 9, *left*. *Left:* before the subtraction of the reprojection of Ω_{DBP} (dotted region) from the data. *Right:* after the subtraction.

We now propose an example configuration without contaminated lines. Other examples are also possible. The

FOV is a cylinder centered on the $\boldsymbol{e}_z$-axis of radius 90mm. The object support Ω_O is a cylinder of same direction with an elliptical base defined by $\{(a\cos\lambda_e + c_o, b\sin\lambda_e), \lambda_e \in [0, 2\pi), a = 80\text{mm}, b = 40\text{mm}, c_o = 20\text{mm}\}$. Its axial extent (in the z-direction) is the interval $[12\text{mm}, 20\text{mm}]$ and the FOV is axially extended on a larger interval (no axial truncation). Finally, concerning S, we have $H = 60$mm and $R = 160$mm. We present this configuration in top view, before and after subtraction of the reprojections from the data, see Fig. 8. It can readily be shown that, with the DBP method, we can reconstruct each point of $\Omega_{\text{DBP}} = \text{FOV} \cap \Omega_O \cap C_S \setminus A$ (the dotted region of Fig. 8, *left*), with $A \overset{\text{def}}{=} \text{conv}(\Omega_O \setminus \text{FOV}) \setminus (\Omega_O \setminus \text{FOV})$ (the orange region of Fig. 9, *left*). However it might be possible to reconstruct some points of the small region A with the M-line methods [12], but this is not the central aim of this article, which is to prove that it is possible to reconstruct Ω_{in}. A 3D illustration is given Fig. 9, *right*.

We see from Fig. 8, *right*, that if there is no contaminated line, the configuration satisfies Tuy condition (there is "no longer any truncation"). Instead of drawing all measured lines (here they are the lines from a source point of S and intersecting the FOV, especially Ω_{in}), we choose to focus on lines intersecting Ω_{in} and Ω_{out} at the same time. These lines delimit two cones and a polyhedron (Fig. 10). We see from Fig. 10 that these cones (and the polyhedron) do not intersect S, so no contaminated lines exist, and thus reconstruction of Ω_{in} is possible.

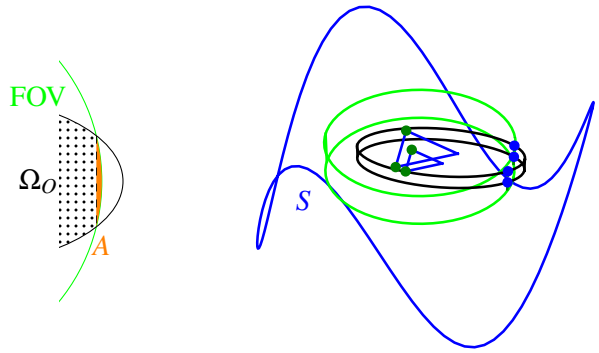

Figure 9: *Left:* Zoom on the right-side of Ω_O: the dotted region is Ω_{DBP}, the orange region is A and the non-dotted (white and orange) region of Ω_O is Ω_{out}. *Right:* The configuration proposed. The FOV is delimited by both green circles, Ω_O by both black ellipses and N_S by the blue triangles (at $z = 12$mm and $z = 20$mm). Dark green and blue dots are used to draw the limit lines of Fig. 10.

4 Simulation

We created a thin cylindrical phantom with an elliptical base as Ω_O, and added some ellipsoid and balls, see Fig. 11. The configuration for the source trajectory and the FOV was the same as described in the previous section. The rectangular detector of 400×430 pixels is at a distance of 290mm from the source. A total of 360 cone-beam projections were simulated along the 3-sin source trajectory. The reconstruction volume consisted of $162 \times 82 \times 8$ voxels (pixels and voxels have a 1-mm side).

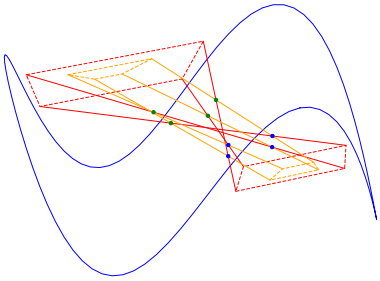

Figure 10: Cones (red) and the polyhedron (orange) delimiting the lines intersecting both Ω_{in} and Ω_{out}. They do not intersect the trajectory S so these lines are not contaminated lines.

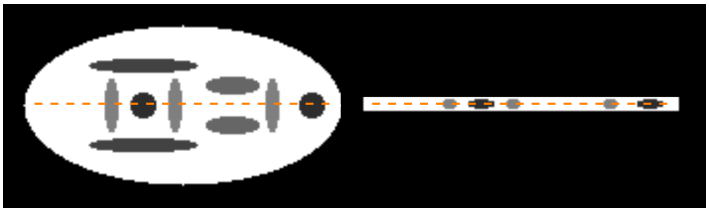

Figure 11: The phantom used for simulations. The orange lines indicate the location of the profile used in Fig. 13. *Left:* Top view. *Right:* Side view.

The objective was to verify the theory that the triangular region N_S could be accurately reconstructed according to the theory established above. The goal was to investigate the results of [6], obtained by an iterative method, so we did not use the DBP method, with the 4 step approach outlined in section 3.1. We just used the conjugate gradient to minimize $\|Rf - p\|_2^2 + \gamma\|\nabla f\|_2^2$ with R the forward projection operator and p the measured projections. With $\gamma = 500$ we performed 60 iterations at which point we considered that convergence had been achieved. Some results are shown Figs. 12 and 13 (with another reconstruction performed without truncation, with a FOV of radius 102mm).

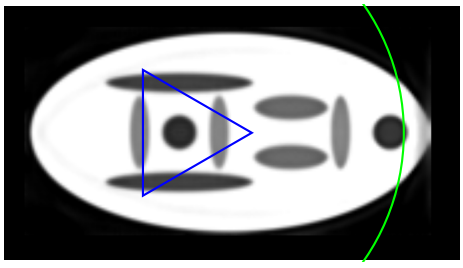

Figure 12: A cross-section at $z = 16$mm of the reconstruction. The green circular arc delimits the FOV and the blue triangle is N_S (for this cross-section).

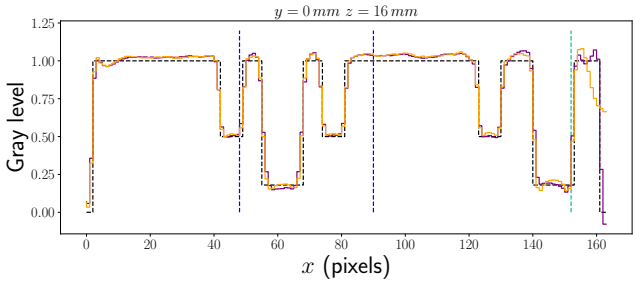

Figure 13: A profile of the reconstruction at $y = 0$mm and $z = 16$mm. The black line is the phantom, the purple line is the reconstruction without truncation and the orange line is the reconstruction with truncation. The dashed green line is the right limit of the FOV (for the reconstruction with truncation) and the dashed blue lines are the limits of N_S.

5 Discussion and conclusion

We have adapted the scheme introduced in [5] for the reverse helix with axial truncation to the 3-sin trajectory with transverse truncation. To our knowledge, it is an original way to manage certain situations of transverse truncation for points lying in the Tuy-Finch region but not lying on a chord.
We performed a simulation (with an iterative method) which showed the same quality of reconstruction in the chord zone as well as the non-chord zone N_S. However, our example only involved very mild transverse truncation. On the other hand, in [6] we presented results showing good quality reconstruction for the same trajectory with much more transverse truncation but without theoretical results to justify it.
The configuration we have presented is rather limited in practice. For example, the object is quite flat. Nevertheless this represents a beginning of a lead, and other more general configurations could be found, for example by considering sub-trajectories of S after subtraction of the reprojections, while guaranteeing Tuy's condition.

Acknowlegdgements The authors would like to thank F.Noo who pointed out the link between articles [5] and [6] and which led to this work. This work was supported by the "Fonds unique interministériel" (FUI) and the European Union FEDER in Auvergne Rhône Alpes (3D4Carm project) and by the ANR (ROIdoré project ANR-17-CE19-0006-01).

References

[1] H. K. Tuy. "Inversion Formula For Cone-Beam Reconstruction". *SIAM Journal on Applied Mathematics* 43.3 (1983), pp. 546–552. DOI: 10.1137/0143035.

[2] D. V. Finch. "Cone Beam Reconstruction with Sources on a Curve". *SIAM Journal on Applied Mathematics* 45.4 (1985), pp. 665–673. DOI: 10.1137/0145039.

[3] X. Pan, D. Xia, Y. Zou, et al. "A unified analysis of FBP-based algorithms in helical cone-beam and circular cone- and fan-beam scans". *Physics in Medicine & Biology* 4349 (2004). DOI: 10.1088/0031-9155/49/18/011.

[4] R. Clackdoyle, F. Noo, F. Momey, et al. "Accurate Transaxial Region-of-Interest Reconstruction in Helical CT?" *IEEE Transactions on Radiation and Plasma Medical Sciences* 1.4 (2017), pp. 334–345. DOI: 10.1109/TRPMS.2017.2706196.

[5] F. Noo, A. Wunderlich, L. Günter, et al. "On the problem of axial data truncation in the reverse helix geometry". *10th International Meeting on Fully Three-Dimensional Image Reconstruction in Radiology and Nuclear Medicine*. 2009, pp. 90–93.

[6] N. Gindrier, R. Clackdoyle, S. Rit, et al. "Cone-beam reconstruction from n-sin trajectories with transversely-truncated projections". *6th International Conference on Image Formation in X-Ray Computed Tomography*. Regensburg, 2020, pp. 46–49.

[7] J. D. Pack, F. Noo, and H. Kudo. "Investigation of saddle trajectories for cardiac CT imaging in cone-beam geometry". *Physics in Medicine and Biology* 49.11 (2004), pp. 2317–2336. DOI: 10.1088/0031-9155/49/11/014.

[8] S. Cho, D. Xia, C. A. Pellizzari, et al. "A BPF-FBP tandem algorithm for image reconstruction in reverse helical cone-beam CT". *Medical Physics* 37.1 (2010), pp. 32–39. DOI: 10.1118/1.3263618.

[9] H. Kudo and T. Saito. "Derivation and Implementation of a Cone-Beam Reconstruction Algorithm for Nonplanar Orbits". *IEEE Transactions on Medical Imaging* 13.1 (1994), pp. 196–211. DOI: 10.1109/42.276158.

[10] M. Defrise and R. Clack. "A Cone-Beam Reconstruction Algorithm Using Shift- Variant Filtering and Cone-Beam Backprojection". 13.1 (1994), pp. 186–195.

[11] R. Clackdoyle and M. Defrise. "Tomographic reconstruction in the 21st century". *IEEE Signal Processing Magazine* July (2010), pp. 60–80.

[12] J. D. Pack, F. Noo, and R. Clackdoyle. "Cone-beam reconstruction using the backprojection of locally filtered projections". *IEEE Transactions on Medical Imaging* 24.1 (2005), pp. 70–85. DOI: 10.1109/TMI.2004.837794.